Effect of ultrasonic irradiation on the preparation of Ag_3PO_4 particles

Yang Yang, Hua Yang, Ruishan Li, Xiangxian Wang

School of Science, Lanzhou University of Technology, Lanzhou 730050, People's Republic of China
E-mail: hyang@lut.cn

Published in Micro & Nano Letters; Received on 17th January 2016; Accepted on 11th February 2016

Herein is investigated the effect of ultrasonic irradiation on the preparation of Ag_3PO_4 particles based on the ion-exchange method. X-ray diffraction, scanning electron microscope, diffuse reflectance spectrum and photoluminescence were used to characterise the products. It is found that the application of ultrasonic irradiation at a frequency of 40 kHz leads to the production of uniform spherical particles with an average size of ~300 nm. However, at a higher ultrasonic frequency of 60 kHz, the prepared sample presents polyhedron-shaped particles in the size range of 6–8 μm, which are constructed from small grains with a size of several hundred nanometres. Without the aid of ultrasonic irradiation, the samples prepared at room temperature or under 50 °C water-bath condition are composed of spherical particles and large-sized agglomerative particles. The photocatalytic activity of Ag_3PO_4 samples was evaluated by degrading rhodamine B (RhB) under simulated sunlight irradiation. Among these samples, the one prepared at 40 kHz exhibits the highest photocatalytic activity, where the degradation percentage of RhB reaches 96% after irradiation for 60 min.

1. Introduction: Semiconductor-based photocatalysis has attracted great interests due to its potential applications in solving current environment and energy problems with solar light [1, 2]. Recently, Ye and co-workers have demonstrated a new type of visible-light driven photocatalyst, silver orthophosphate (Ag_3PO_4) with a bandgap energy of ~2.4 eV, that exhibits powerful photocatalytic capabilities for the decomposition of organic compounds and O_2 evolution from water splitting under visible light irradiation [3–6]. It is particularly interesting that Ag_3PO_4 has a high separation of photoexcited electrons (e^-) and holes (h^+) as well as a high quantum efficiency up to 90% at wavelengths above 420 nm [3, 4]. In most cases, the particle size and morphology of a photocatalyst plays an important role in its photocatalytic activity. For example, Jiao *et al.* [7] demonstrated that concave trisoctahedral Ag_3PO_4 microcrystals enclosed by {221} and {332} facets exhibited much higher photocatalytic activity than cubic Ag_3PO_4 crystals. Furthermore, small-sized photocatalyst is expected to achieve superior photocatalytic activity since it can provide a large specific area for the photocatalytic reaction. Generally, the particle size/morphology of the photocatalyst as well as its properties depends on the preparation process to a great extent.

Ultrasonic wave propagating in liquid can generate acoustic cavitation, which involves the processes of nucleation, growth and implosion of cavitation bubbles. The violent implosion of cavitation bubbles results in the production of local high temperature (>5000 K) and high pressure (>1000 atm), and furthermore the temperature has a high cooling rate (>10^{10} K/s) [8]. The extreme conditions have important effects on chemical reactions, consequently leading to the crystallisation of unique particles [9–11]. Recently, ion-exchange method, hydrothermal method, electrochemical oxidisation method and colloidal synthesis have been extensively used to prepare Ag_3PO_4 particles [5, 12–22]. However, there has been little work concerned with the effect of ultrasonic irradiation on the preparation of Ag_3PO_4 particles [23]. Herein we report the ion-exchange synthesis of Ag_3PO_4 particles with the aid of ultrasonic irradiation.

2. Experimental: All raw materials and chemical reagents used in this study are of analytical grade without further purification. In a typical synthesis process, 0.003 mol of $AgNO_3$, 0.001 mol of $NaH_2PO_4{\cdot}2H_2O$ and 0.002 mol of NaOH were dissolved in 20, 10 and 10 ml of distilled water with the aid of magnetic stirring for 10 min, respectively. The NaOH solution was added by drops into the $NaH_2PO_4{\cdot}2H_2O$ solution under vigorous magnetic stirring to form a mixed solution. The $AgNO_3$ solution was placed in an ultrasonic bath, to which was then added the mixed solution drop by drop. The reaction solution was ultrasonically irradiated at an ultrasonic frequency of 40 or 60 kHz. The ultrasonic bath temperature was controlled at 50 °C by circulating running water through the ultrasonic bath. After 1 h of reaction, a yellow precipitate was formed. The precipitate was collected and washed with distilled water and absolute ethanol for several times, and then submitted to drying at 60 °C for 12 h, finally yielding Ag_3PO_4 particles. The samples prepared at 40 and 60 kHz are termed as S1 and S2, respectively. For comparison, two other Ag_3PO_4 samples were also prepared via the ion-exchange method without the aid of ultrasonic irradiation: one prepared at room temperature (termed as S3) and the other prepared under water-bath condition at 50 °C (termed as S4).

The phase purity and crystal structure of the as-prepared samples was characterised by powder X-ray diffraction (XRD) with Cu-Kα radiation ($\lambda = 1.5406$ Å). The particle morphology and size of the samples was investigated by a field-emission scanning electron microscope (SEM). The ultraviolet (UV)–visible diffuse reflectance spectrum (DRS) of the samples was measured using a UV–visible spectrophotometer with an integrating sphere attachment. The photoluminescence (PL) spectrum of the samples was measured at a fluorescence spectrophotometer with excitation wavelength of 444 nm.

The photocatalytic activity of the samples was investigated by the degradation of organic dye rhodamine B (RhB) in aqueous solution under simulated sunlight irradiation from a 200 W xenon lamp. The initial RhB concentration was 5 mg l^{-1} and the Ag_3PO_4 loading was 0.02 g in 100 ml of RhB solution. Before illumination, the suspension was magnetically stirred for 30 min in the dark to reach the adsorption–desorption equilibrium of RhB onto the catalyst particle surface. During the photocatalysis process, 2.5 ml of the reaction solution was pipetted out at regular time intervals and centrifuged at 4000 r min^{-1} for 10 min to remove the catalyst. The RhB concentration was determined by measuring the absorbance of the solution at $\lambda = 554$ nm using an UV–visible spectrophotometer. The degradation percentage is defined as $(C_0 - C_t)/C_0 \times 100\%$, where C_0 is the initial RhB concentration and C_t is the RhB concentration after photocatalysis for time t.

3. Results and discussion: Fig. 1 shows the XRD patterns of the as-prepared Ag_3PO_4 samples, where S1, S2, S3 and S4 represent

the samples prepared at an ultrasonic frequency of 40 kHz and a temperature of 50 °C, prepared at 60 kHz and 50 °C, prepared without the aid of ultrasonic irradiation and at room temperature, and prepared without the aid of ultrasonic irradiation and under 50 °C water-bath condition, respectively. The standard XRD line pattern for Ag_3PO_4 cubic structure (Joint Committee on Powder Diffraction Standards (JCPDS) Card No. 06-0505) is also given in Fig. 1. It is clear that all diffraction peaks of the samples are in good agreement with those in the JCPDS Card No., and no diffraction peaks assignable to other secondary phases are detected. This indicates that the four samples crystallise in a pure cubic phase.

Figs. 2*a*–*d* show the SEM images of samples S1–S4, respectively. From Fig. 2*a* one can see that the application of ultrasonic irradiation at a frequency of 40 kHz leads to the production of regular spherical particles without any adhesive or agglomerative behaviour. The particles have a narrow diameter distribution with an average size of ~300 nm. However, at a higher ultrasonic frequency of 60 kHz, the resulted sample presents polyhedron-shaped particles in the size range of 6–8 μm, which are constructed from small grains with a size of several nanometres (see Fig. 2*b*). The effect of ultrasonic irradiation on the particle morphology can be possibly interpreted as follows. When the reaction solution is exposed to the ultrasound irradiation, the induced acoustic cavitation results in local high temperature, pressure and cooling rate [8], and the extreme conditions have a dependence on the ultrasonic frequency. At a proper frequency (here 40 kHz), the generated extreme conditions can drive a variety of chemical reactions, thus producing regular Ag_3PO_4 particles with narrow size distribution and minor aggregation. However, at a high ultrasonic frequency (here 60 kHz), the number of cavitation elements is greatly increased and furthermore it brings about great enhancement in the diffusion mass transfer [24]. As a result, the formed small grains tend to agglomerate, thus forming large-sized agglomerative particles. From Figs. 2*c* and *d* it is seen that without the aid of ultrasonic irradiation, the samples prepared at room temperature or under 50 °C water-bath condition mainly consist of spherical particles in an average size of ~300 nm and large-sized agglomerative particles with a size of several hundred micrometres.

This indicates that the absence of ultrasonic irradiation in the present experiments cannot allow the production of uniform spherical Ag_3PO_4 particles.

Fig. 3*a* shows the UV–visible diffuse reflectance spectra of Ag_3PO_4 samples, and Fig. 3*b* gives the corresponding first derivative of the reflectance (R) with respect to wavelength λ (i.e. $dR/d\lambda$). It is seen that samples S1, S3 and S4 have a similar absorption peak at 498 nm. The absorption peak is suggested to be attributed to the electron transition from valence band to conduction band, from which the bandgap energy E_g of the three samples is obtained to be 2.49 eV. Sample S2 has a slightly higher absorption peak at 510 nm, from which its bandgap energy is obtained to be 2.43 eV. The observation of relatively small bandgap energy for sample S2 is due to the fact that this sample is composed of large-sized agglomerative particles. Generally, the bandgap energy of semiconductor particles has a dependence on their size, and exhibits a decreasing trend with increasing the particle size [25]. In addition, an obvious light absorbance centred around 450 nm is observed for samples S1, S3 and S4. The absorption band is attributed to the surface plasmon resonance (SPR) effect of Ag nanoparticles [26]. This indicates that Ag nanoparticles are formed onto the surface of the spherical Ag_3PO_4 particles; however, their number is very small since no diffraction peaks assignable to Ag particles are detected in the XRD patterns (see Fig. 1). For sample S2, no obvious SPR signal of Ag nanoparticles is observed, implying almost no Ag nanoparticles produced onto the large-sized agglomerative particles.

Fig. 4 shows the PL spectra of Ag_3PO_4 samples. Two emission bands separately centred around 617 and 668 nm are visible in the PL spectra. The emission band at the lower wavelength is possibly originated from the recombination of electrons and holes. It is obvious that samples S1, S3 and S4 exhibit a higher intensity of the peak at 617 nm compared with sample S2. The effect of interfacial electron transfer can be considered to account for this phenomenon. It is noted that for samples S1, S3 and S4, Ag nanoparticles are formed onto the spherical Ag_3PO_4 particles, as evidenced by the DRS spectra (Fig. 3). Since the Fermi level of Ag [+0.4 V against normal hydrogen electrode (NHE)] is negative to the conduction band potential of Ag_3PO_4 (+0.45 V against NHE) [3, 26], the electron transfer possibly occurs from Ag to Ag_3PO_4 from a thermodynamical point of view. Due to the carrier transfer process, the recombination rate of electrons and holes is expected to be increased, thus leading to an intensive emission band at 617 nm. A similar observation and interpretation was made in the case of the Ag–ZnO system [27].

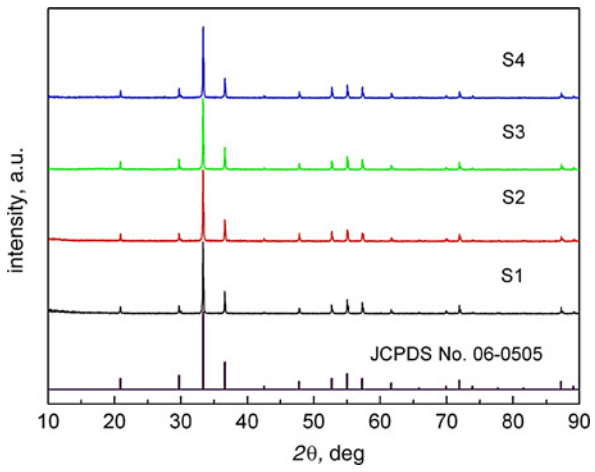

Fig. 1 *XRD patterns of the as-prepared Ag_3PO_4 samples. S1 – the sample prepared at an ultrasonic frequency of 40 kHz and a temperature of 50 °C, S2 – the sample prepared at 60 kHz and 50 °C, S3 – the sample prepared without the aid of ultrasonic irradiation and at room temperature, S4 – the sample prepared without the aid of ultrasonic irradiation and under 50 °C water-bath condition*

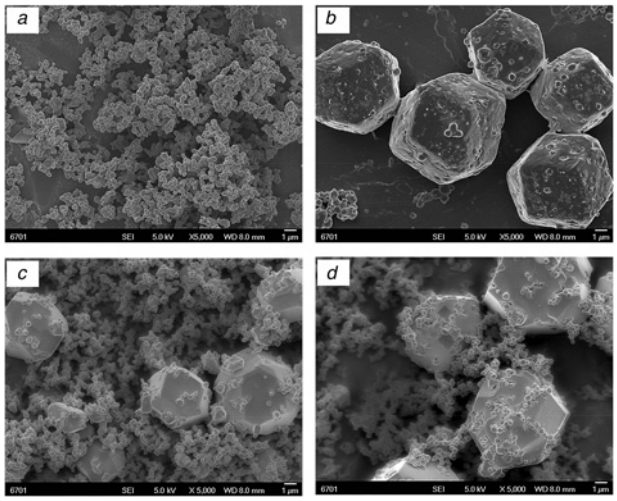

Fig. 2 *SEM images of Ag_3PO_4 samples*
a S1
b S2
c S3
d S4

doi: 10.1049/mnl.2015.0577

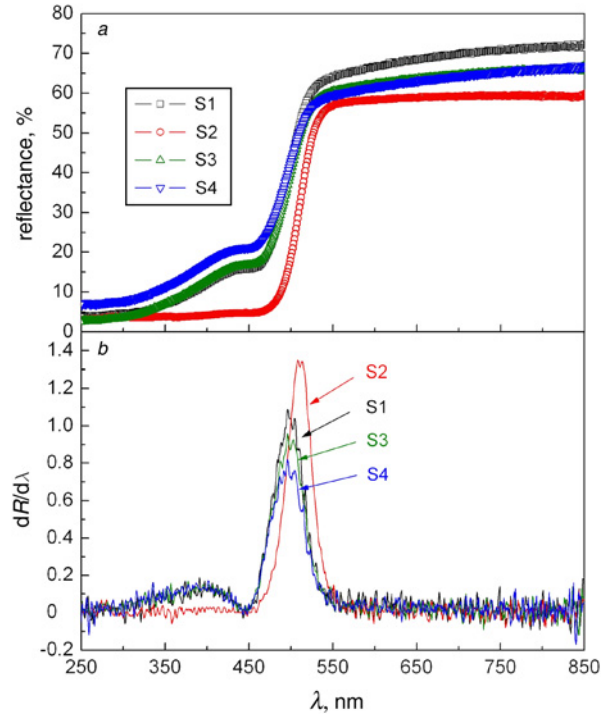

Fig. 3 *Optical properties of Ag_3PO_4 samples*
a UV–visible diffuse reflectance spectra of Ag_3PO_4 samples
b Corresponding first derivative of the reflectance (R) with respect to wavelength λ (i.e. d*R*/d*λ*)

Fig. 5 shows the adsorption of RhB onto Ag_3PO_4 samples and its photocatalytic degradation over the samples under simulated sunlight irradiation as a function of irradiation time (*t*), along with the blank experiment result. In the absence of the photocatalyst, RhB appears to be stable under simulated sunlight irradiation and its degradation is almost negligible after 60 min of exposure (only 1%). In the absence of light irradiation, the adsorption percentage of RhB onto the four Ag_3PO_4 samples is about 12–17% after 30 min of adsorption, indicating that these samples have a moderate adsorption toward RhB. The photocatalytic experiments reveal that the four samples have different photocatalytic activities. After 60 min of photocatalysis reaction, the degradation percentages of RhB are about 96, 68, 77 and 80% by using the samples S1, S2, S3 and S4 as the photocatalyst, respectively. It is obvious that the sample S1, which was prepared with the aid of ultrasonic irradiation at 40 kHz, exhibits the highest photocatalytic activity. This is due to the fact that this sample is composed of regular and uniform

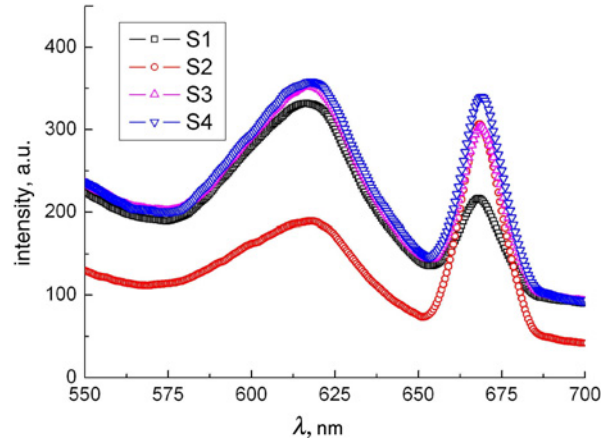

Fig. 4 *PL spectra of Ag_3PO_4 samples*

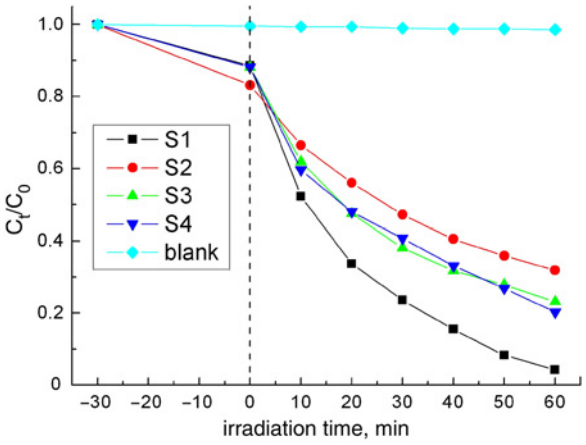

Fig. 5 *Adsorption of RhB onto Ag_3PO_4 samples and its photocatalytic degradation over the samples under simulated sunlight irradiation as a function of irradiation time (t), along with the blank experiment result*

particles without any aggregation, thus can provide a large specific area for the photocatalytic reaction.

4. Conclusion: Ag_3PO_4 particles were prepared via an ion-exchange method, where the effect of ultrasonic irradiation on the morphology of products was investigated. SEM observation demonstrates that the sample (S1) prepared with the aid of ultrasonic irradiation at 40 kHz is composed of uniform spherical particles with an average size of ∼300 nm. However, the sample (S2) prepared at a higher ultrasonic frequency of 60 kHz presents polyhedron-shaped particles in the size range of 6–8 μm, which are constructed from small grains with a size of several hundred nanometres. In the absence of ultrasonic irradiation, the samples prepared at room temperature (S3) or under 50 °C water-bath condition (S4) exhibit non-uniform particle morphology. Basides the spherical particles of 300 nm in size, a number of large-sized agglomerative particles are also observed for the two samples. All the samples crystallise in a pure cubic phase. Samples S1, S3 and S4 have a similar bandgap energy of 2.49 eV, while sample S2 has a slightly smaller bandgap energy of 2.43 eV. PL spectra suggest a relatively higher recombination rate of electrons and holes for samples S1, S3 and S4, which is due to the formation of Ag nanoparticles onto the surface of Ag_3PO_4 particles. The photocatalytic experiments reveal that sample S1 has the highest photocatalytic activity and the degradation percentage of RhB reaches 96% after irradiation for 60 min.

5. Acknowledgments: This work was supported by the National Natural Science Foundation of China (grant no. 51262018), the Fundamental Research Funds for Universities of Gansu Province (grant no. 056003) and the Hongliu Outstanding Talents Foundation of Lanzhou University of Technology (grant no. J201205).

6 References

[1] Mills A., Davies R.H., Worsley D.: 'Water purification by semiconductor photocatalysis', *Chem. Soc. Rev.*, 1993, **22**, pp. 417–425
[2] Hoffmann M.R., Martin S.T., Choi W., *et al.*: 'Environmental applications of semiconductor photocatalysis', *Chem. Rev.*, 1995, **95**, pp. 69–96
[3] Yi Z., Ye J., Kikugawa N., *et al.*: 'An orthophosphate semiconductor with photooxidation properties under visible-light irradiation', *Nat. Mater.*, 2010, **9**, pp. 559–564
[4] Bi Y., Ouyang S., Umezawa N., *et al.*: 'Facet effect of single-crystalline Ag_3PO_4 sub-microcrystals on photocatalytic properties', *J. Am. Chem. Soc.*, 2011, **133**, pp. 6490–6492

[5] Hu H., Jiao Z., Yu H., *ET AL.*: 'Facile synthesis of tetrahedral Ag_3PO_4 submicro-crystals with enhanced photocatalytic properties', *J. Mater. Chem. A*, 2013, **1**, pp. 2387–2390
[6] Umezawa N., Shuxin O., Ye J.: 'Theoretical study of high photocatalytic performance of Ag_3PO_4', *Phys. Rev.*, 2011, **83**, pp. 035202
[7] Jiao Z., Zhang Y., Yu H., *ET AL.*: 'Concave trisoctahedral Ag_3PO_4 microcrystals with high-index facets and enhanced photocatalytic properties', *Chem. Commun.*, 2013, **49**, pp. 636–638
[8] Suslick K.S.: 'The sonochemical hot spot', *J. Acoust. Soc. Am.*, 1991, **89**, pp. 1885–1886
[9] Hanifehpour Y., Safarifard V., Morsali A., *ET AL.*: 'Sonochemical syntheses of two new flower-like nano-scale high coordinated lead (II) supramolecular coordination polymers', *Ultrason. Sonochem.*, 2015, **23**, pp. 282–288
[10] Yusof N.S.M., Ashokkumar M.: 'Sonochemical synthesis of gold nanoparticles by using high intensity focused ultrasound', *Chem. Phys. Chem.*, 2015, **16**, pp. 775–781
[11] Yao K., Dong Y.Y., Bian J., *ET AL.*: 'Understanding the mechanism of ultrasound on the synthesis of cellulose/$Cu(OH)_2$/CuO hybrids', *Ultrason. Sonochem.*, 2015, **24**, pp. 27–35
[12] Botelho G., Sczancoski J.C., Andres J., *ET AL.*: 'Experimental and theoretical study on the structure, optical properties, and growth of metallic silver nanostructures in Ag_3PO_4', *J. Phys. Chem. C*, 2015, **119**, pp. 6293–6306
[13] Kumar S., Surendar T., Shanker V.: 'Template-free and eco-friendly synthesis of hierarchical Ag_3PO_4 microcrystals with sharp corners and edges for enhanced photocatalytic activity under visible light', *Mater. Lett.*, 2014, **123**, pp. 172–175
[14] Liu J.K., Luo C.X., Wang J.D., *ET AL.*: 'Controlled synthesis of silver phosphate crystals with high photocatalytic activity and bacteriostatic activity', *CrystEngComm*, 2012, **14**, pp. 8714–8721
[15] Hatakeyama K., Okuda M., Kuki T., *ET AL.*: 'Removal of dissolved humic acid from water by photocatalytic oxidation using a silver orthophosphate semiconductor', *Mater. Res. Bull.*, 2012, **47**, pp. 4478–4482
[16] Wang H., He L., Wang L., *ET AL.*: 'Facile synthesis of Ag_3PO_4 tetrapod microcrystals with an increased percentage of exposed {110} facets and highly efficient photocatalytic properties', *CrystEngComm*, 2012, **14**, pp. 8342–8344
[17] Li X.Z., Wu K.L., Dong C., *ET AL.*: 'Size-controlled synthesis of Ag_3PO_4 nanorods and their high-performance photocatalysis for dye degradation under visible-light irradiation', *Mater. Lett.*, 2014, **130**, pp. 97–100
[18] Lou Z., Huang B., Wang Z., *ET AL.*: 'Fast-generation of Ag_3PO_4 concave microcrystals from electrochemical oxidation of bulk silver sheet', *CrystEngComm*, 2013, **15**, pp. 5070–5075
[19] Guan X., Shi J., Guo L.: 'Ag_3PO_4 photocatalyst: hydrothermal preparation and enhanced O_2 evolution under visible-light irradiation', *Int. J. Hydrog. Energy*, 2013, **38**, pp. 11870–11877
[20] Liu Y.P., Fang L., Lu H.D., *ET AL.*: 'One-pot pyridine-assisted synthesis of visible-light-driven photocatalyst Ag/Ag_3PO_4', *Appl. Catal. B, Environ.*, 2012, **115–116**, pp. 245–252
[21] Wang J., Teng F., Chen M., *ET AL.*: 'Facile synthesis of novel Ag_3PO_4 tetrapods and the {110} facets-dominated photocatalytic activity', *CrystEngComm*, 2013, **15**, pp. 39–42
[22] Khan A., Qamar M., Muneer M.: 'Synthesis of highly active visible-light-driven colloidal silver orthophosphate', *Chem. Phys. Lett.*, 2012, **519**, pp. 54–58
[23] Dong P.Y., Wang Y.H., Li H.H., *ET AL.*: 'Shape-controllable synthesis and morphology-dependent photocatalytic properties of Ag_3PO_4 crystals', *J. Mater. Chem. A*, 2013, **1**, pp. 4651–4656
[24] Trabelsi F., Ait-Lyazidi H., Ratsimba B., *ET AL.*: 'Oxidation of phenol in wastewater by sonoelectrochemistry', *Chem. Eng. Sci.*, 1996, **51**, pp. 1857–1865
[25] Wang S.F., Yang H., Xian T., *ET AL.*: 'Size-controlled synthesis and photocatalytic properties of $YMnO_3$ nanoparticles', *Catal. Commun.*, 2011, **12**, pp. 625–628
[26] Xian T., Yang H., Di L.J., *ET AL.*: 'Enhanced photocatalytic activity of $SrTiO_3$ particles by surface decoration with Ag nanoparticles for dye degradation', *Phys. Scr.*, 2015, **90**, p. 055801
[27] Zhai H.J., Wang L.J., Han D.L., *ET AL.*: 'Facile one-step synthesis and photoluminescence properties of Ag–ZnO core–shell structure', *J. Alloys Compd.*, 2014, **600**, pp. 146–150

doi: 10.1049/mnl.2015.0577